Published in final edited form as:
Mol Microbiol. 2013 May ; 88(4): 664–672. doi:10.1111/mmi.12203.

Architecture and assembly of the Gram-positive cell wall

Morgan Beeby[1,2], **James C. Gumbart**[3,4], **Benoît Roux**[3,5], and **Grant J. Jensen**[1,*]

[1]California Institute of Technology and Howard Hughes Medical Institute, 1200 E. California Blvd, Pasadena, CA 91125, USA

[3]Biosciences Division, Argonne National Laboratory, Argonne, Illinois 60439

[5]Department of Biochemistry and Molecular Biology and Gordon Center for Integrative Science, The University of Chicago, Chicago, Illinois 60637

Abstract

The bacterial cell wall is a mesh polymer of peptidoglycan – linear glycan strands crosslinked by flexible peptides – that determines cell shape and provides physical protection. While the glycan strands in thin "Gram-negative" peptidoglycan are known to run circumferentially around the cell, the architecture of the thicker "Gram-positive" form remains unclear. Using electron cryotomography, here we show that *Bacillus subtilis* peptidoglycan is a uniformly dense layer with a textured surface. We further show it rips circumferentially, curls and thickens at free edges, and extends longitudinally when denatured. Molecular dynamics simulations show that only atomic models based on the circumferential topology recapitulate the observed curling and thickening, in support of an "inside-to-outside" assembly process. We conclude that instead of being perpendicular to the cell surface or wrapped in coiled cables (two alternative models), the glycan strands in Gram-positive cell walls run circumferentially around the cell just as they do in Gram-negative cells. Together with providing insights into the architecture of the ultimate determinant of cell shape, this study is important because Gram-positive peptidoglycan is an important antibiotic target crucial to the viability of several important rod-shaped pathogens including *Bacillus anthracis*, *Listeria monocytogenes*, and *Clostridium difficile*.

Keywords

Gram-positive peptidoglycan architecture; electron cryo-tomography; molecular dynamics; hybird methods; biological self-organization

Introduction

A key conceptual hurdle in contemporary biology is understanding how the interactions between nano-scale proteins produce micro-scale order. Bacterial proteins, for instance, endow cells with a consistent cell shape by assembling a multi-gigadalton sacculus of peptidoglycan just outside the cytoplasmic membrane. Inflation of this sacculus with its other embedded macromolecules (the "cell wall") by cellular turgor pressure produces the

*To whom correspondence should be addressed: jensen@caltech.edu Phone: (626) 395 8827 Fax: (626) 395 5730.
[2]Current address: Department of Life Sciences, Imperial College London, South Kensington Campus, London SW7 2AZ, UK
[4]Current address: School of Physics, Georgia Institute of Technology, Atlanta, GA 30332

Concise description: The architecture of Gram-positive peptidoglycan is still not established, despite decades of research, partially due to a lack of methods to directly visualize it because of it's intermediate size. Here we use electron cryo-tomography to image Gram-positive peptidoglycan in 3-D, and combine this with molecular dynamics simulations to bridge scales. Multiple lines of evidence from our work, together with multiple lines of evidence by previous researchers, strongly support the model in which glycan strands run circumferentially around the long-axis of the cell.

characteristic spherical, rod, helical, flat wave, or star shapes seen in different species(Young 2006). While two different classes of cell wall are clearly distinguished (thin "Gram-negative" and thick "Gram-positive"), the chemical structure of peptidoglycan(W Vollmer, Blanot, and De Pedro 2008) is conserved: relatively rigid linear polymers of the dissacharide N-acetylglucosamine – N-acetylmuramic acid are crosslinked by non-ribosomally synthesized peptides attached to the lactate residue of N-acetylmuramic acid. The families of proteins responsible for peptidoglycan assembly are also conserved, including the periplasmic penicillin-binding proteins (PBPs) that both polymerize and crosslink the linear glycan strands(Lovering, Safadi, and Strynadka 2012). In almost all rod-shaped bacteria, the bacterial actin homolog MreB is also conserved and essential for normal cell morphology. Depletion of MreB leads to cell swelling and eventual lysis(Wachi and Matsuhashi 1989), but the nature of its crucial function in maintaining wild-type rod shape remains enigmatic.

While the chemical nature of peptidoglycan is understood, the non-crystalline arrangement of components(Burge, Fowler, and Reaveley 1977) has made visualizing its architecture difficult. Electron cryo-tomography (ECT) of rod-shaped Gram-negative sacculi, however, revealed long skinny densities running mostly circumferentially around the long-axis of the cell(Gan, Chen, and Jensen 2008). These densities were likely individual glycan strands, strongly supporting the model that glycan strands run around the long axis of the cell(Verwer et al. 1978). The arrangement of peptidoglycan in the considerably thicker cell wall of Gram-positive rod-shaped bacteria is still controversial(Waldemar Vollmer and Seligman 2010), however, with three mutually exclusive models described in the literature. In the circumferential (or "layered", although the presence of discrete layers is unlikely) model(Ghuysen 1968), glycan strands are also proposed to run circumferentially around the long axis of the cell. In the perpendicular (or "scaffold") model, glycan strands are oriented perpendicular to the cell in a hexagonal lattice(Dmitriev, Toukach, and Ehlers 2005; Meroueh et al. 2006). Finally, AFM studies of fragmented *Bacillus subtilis* peptidoglycan gave rise to a "coiled cable" model in which bundles of glycan strands coil tightly to form 50-nm-diameter cables which in turn wrap around the cell(Hayhurst et al. 2008). Models that feature glycan strands running parallel to the long-axis of the cell have not been seriously considered because it is unclear how such sacculi could elongate to allow cell growth. Previous 2-D electron cryo-microscopy projection images of cryo-sectioned whole *B. subtilis* cells showing a homogenous density throughout the cell wall were inconsistent with the coiled cable model, but could not distinguish between the circumferential and perpendicular models(Matias and Beveridge 2005).

Encouraged by our earlier success imaging Gram-negative sacculi(Gan, Chen, and Jensen 2008), here we used ECT to investigate the architecture of the Gram-positive peptidoglycan sacculus of the model organism *B. subtilis*. In ECT, plunge-frozen biological samples are imaged in their native growth media or storage buffer. A series of 2-D projection images of the still-vitrified sample are acquired in an electron microscope while the sample is incrementally rotated about an axis. The 2-D images are then used to calculate a 3-D reconstruction of the sample with a resolution typically sufficient to discern individual macromolecular complexes(Chen et al. 2010). Because ECT produces 3-D reconstructions, we were able to make a number of key observations not accessible in 2-D projection images, which, with the aid of computational modeling and molecular dynamics simulations, can only be explained by the circumferential model. We conclude that the basic architecture of peptidoglycan (circumferential glycans) is universally conserved across Gram-negative and Gram-positive rod-shaped bacteria.

Results

To visualize the architecture of Gram-positive peptidoglycan, we initially imaged whole cells. Because wildtype *B. subtilis* cells are too thick for ECT(Gan and Jensen 2012), to avoid the need for cryosectioning we imaged a Δ*ponA* mutant as described in more detail in the accompanying paper (Tocheva and Jensen et al., "Peptidoglycan transformations during Bacillus subtilis sporulation", co-submitted). Tomographic slices showed a thick (~30nm) layer of peptidoglycan encapsulating the cell (Figure 1A). The peptidoglycan was uniformly dense throughout with no internal structure. While the inner surface was smooth and flush with the membrane, the outer surface was rougher.

Next, purified we purified and imaged both intact and fragmented sacculi. Purified sacculi flattened in the plane of vitreous ice (Figure 1B) and did not display structures resembling coiled cables on their inner surface, although circumferentially-oriented textures remained visible (Figure 1C,D). Mechanically sheared sacculi further confirmed this (Figure 2A), and tears were observed to be almost exclusively circumferential. Strikingly, free sheets of peptidoglycan curled tightly, wrapping into concentric curls. Patches that were still connected to the original sacculus (Figure 2A,B) revealed that the outer surface of the original sacculus always faced inwards (towards the axis) in the curls.

In order to compare this observed curling with the predictions of the models, we simulated the assembly of Gram-positive sacculi following different assembly schemes and then allowed the structures to relax as if freed from the sacculus by shearing. Following the proposed inside-to-outside assembly pathway in which new glycan chains are deposited on the inner face and broken down by secreted autolysins on the outer face(Koch and Doyle 1985), a circumferential model was initiated with a row of glycan strands spaced ~2 nm apart (Figure 3A), crosslinked by peptides. These strands were then migrated outward and further apart laterally (within the plane of the sacculus) as new glycan strands were added below. New glycan strands were added in random positions, but always in the same orientation as the original row (see Methods). As new glycan strands were added, additional crosslinks were formed between adjacent strands both laterally and to the next higher layer. As older glycan strands were pushed outwards and further apart laterally, peptide crosslinks stretched, creating lateral and vertical tension that pulled the outer, top glycans toward the inner face, packing them more tightly in the vertical direction. As a result the density of the sacculus remained roughly constant throughout, even though the glycans at the top were widely separated laterally. This process was continued until the patch of peptidoglycan was ~5 glycan strands deep and twice as wide along the cell long axis, akin to a single growth cycle of the bacterium(Koch and Doyle 1985).

Two different assembly schemes - "all-at-once" and "incremental" - were then used to produce perpendicular models. To produce the all-at-once model (as originally proposed(Dmitriev, Toukach, and Ehlers 2005)), a set of equally long glycan strands were placed perpendicular to the cell surface, spaced 2 nm apart (see Figure 3B). These were then crosslinked by peptides and slowly pulled apart laterally. This stretching continued until the patch doubled in length.

Next, the considerable evidence for progressive inside-to-outside migration of peptidoglycan(Koch and Doyle 1985) lead us to assemble an alternative, "incremental" perpendicular model. Again glycan strands were placed perpendicular to the cell surface spaced 2 nm apart and crosslinked by peptides, but this time as the existing glycans were stretched apart laterally, new dissacharides were added from the inside surface both to the ends of existing perpendicular strands and as the beginnings of new perpendicular strands. As a result, glycan density decreased towards the exterior of the sacculus, and peptide

crosslinks were under higher tension the further they migrated from the cell surface (Figure 3C). Three cycles of stretching and addition were applied to the lattice until it elongated to twice its original length. In all cases the inner surface was held in place to reflect its interaction with enzymes on the surface of the inner membrane and the maximum extension of peripheral peptides. No coiled cable models were simulated, since the aforementioned experiments and molecular biological considerations had already refuted this model.

After the three different models were constructed and their growth simulated, the relaxation of each was simulated simply by removing all external constraints. By decoupling the cell-wall fragment from its assumed neighbors (the “periodic box”), it became finite and, thus, free to deform in any dimension (see Figure 3, Supplemental Figures S1–S3). We allowed the fragments to relax for 10–15 ns. The circumferential model curled immediately (Figure 3A); the final radius of curvature was estimated to be 20–35 nm, roughly agreeing with that observed in sacculus fragments in the tomograms as shown in Figure 2, although direct comparisons are not possible as for the sake of reducing computational time our simulated fragments are considerably thinner (~10 nm, Figure 3) than real peptidoglycan sheets (~30 nm, Figure 4). In addition to curling, the peptidoglycan patch with circumferential architecture also thickened. To quantitate this, we imposed a grid of 40 x 40 Å cells in the plane of the peptidoglycan sheet, and for each cell chose the most distal pair of dissacharides (i.e, choosing one on each “face” of the peptidoglycan layer). Using this approach, we measured 45 glycan pairs for the circumferential model, observing thickening of up to ~25% (an average increase in thickness of 13% +/− 8% after discarding the peripheral two strips of glycan pairs due to edge effects) in a single molecular dynamics simulation (Figure 3A, 4A). The all-at-once perpendicular model, in which glycan strand density was constant across the height of the peptidoglycan, did not curl (Figure 3B) or thicken (slightly compacting by -3% +/− 2% thickness change) as assessed by 38 glycan pairs. The incremental perpendicular model (with decreasing glycan density towards the top), exhibited slight curling with a radius of curvature between 50 and 60 nm (Figure 3C), but did not thicken (slightly compacting by −2% +/− 1%) as measured using 45 glycan pairs.

Intrigued by this difference in thickening, we re-examined the experimental data on real sacculi to see if the same behavior was present. We inspected strained peptidoglycan (i.e., imaged in the sidewall of intact sacculi) and relaxed peptidoglycan (i.e., imaged in the curls observed in fragmented peptidoglycan) in cryotomograms. Thicknesses were measured and compared from the strained and relaxed peptidoglycan (Figure 4B). Average shortest distances between the inner to outer faces were measured for multiple lengths of peptidoglycan, and plotted (Figure 4C). In agreement with the simulations of the circumferential model, relaxed peptidoglycan was seen to be ~20% thicker (35.4 nm +/− 8.2 nm) than peptidoglycan under tension (29.8 nm +/− 7.0 nm), providing constraints regarding the possible underlying molecular arrangement of glycans and peptides.

Finally, previous studies demonstrating that sacculi expand under denaturing conditions(Koch and Woeste 1992) and our observation of intra-peptide interactions (peptide condensation) in the molecular dynamics simulations led us to image sacculi in different denaturing conditions. Because denaturating conditions will affect any peptide secondary structure present, but will not affect the relatively rigid conformation of the linear glycan polymers, we reasoned that denaturation of sacculi would provide further constraints on possible underlying molecular architectures. To examine the effects of denaturation upon intact sacculi, a total of 287 sacculi were imaged at pH 7.0 and 109 sacculi were imaged at pH 10.5 in 6M urea to disrupt noncovalent interactions. As expected, sacculi dilated upon denaturation. Denatured sacculi were significantly longer than those at pH 7.0 (with an increase in average length of 20%, or 1.0 μm: 5.9 μm +/− 1.1 μm for denatured sacculi versus 4.9 μm +/− 1.1 μm for undenatured), significant by a two-tailed T-test. No increase

in width, however, was observed (1.31 μm +/− 0.1 μm versus 1.33 μm +/1 0.1 μm for denatured and undenatured, respectively) (Figure 5), suggesting that the peptide crosslinks, which elongate under denaturing conditions, are oriented parallel to the long cell axis. It is not possible to directly compare this elongation to the individual elongation of an isolated peptide bond (which is 4 nm) because the connectivity of the peptidoglycan meshwork is unknown and may play a major role in restricting elongation (for example, peptide crosslinks perpendicular to the plane of the peptidogylcan sheet will limit lateral elongation more than peptide crosslinks in the plane of the sheet).

Discussion

Three models for the basic architecture of the cell wall of Gram-positive rod-shaped cells have been proposed. The most recent is the “coiled cable” model, which posits that bundles of glycan strands coil tightly into 50 nm “cables” that then wrap around cells circumferentially. The main evidence for this model was AFM images of fragmented sacculi, which suggested the outer surface of the cell wall was smooth, but the inner surface was corrugated by ~50 nm circumferential ridges(Hayhurst et al. 2008). Whereas AFM reveals only surfaces, ECT enables full 3-D visualization, including interiors. Using ECT, we saw that the cell wall is a uniformly dense fabric (not a row of hollow coiled cables) with surfaces roughened by circumferential furrows (on the same scale of ~50 nm). Both intact cell walls and purified sacculi were also too thin (30 nm in both cases) to harbor round 50 nm cables. Fragmenting sacculi resulted in circumferential tears and patches, but not 50 nm cables. It is also known that Gram-positive peptidoglycan thickness can be modulated, becoming both thicker(Hanaki et al. 1998), and thinner(Cheng and Costerton 1977), at odds with discrete coiled cables that would always have substantial diameters due to the stiffness of glycan strands. It is further unclear how peptidoglycan cables could be assembled prior to incorporation into the sacculus in the absence of a consistent and large periplasmic space, and no 50 nm gaps were seen in cell walls or sacculi corresponding to the insertion points of new cables. Finally, large and new complex protein machinery would be required in Gram-positive species but not Gram-negative species to bundle and coil glycan strands into cables, and then wrap those coiled cables around the cell; however, no such special machinery has been identified. We therefore reject the coiled cable model, and suggest instead that the corrugations that were previously interpreted as cables are the circumferential furrows seen here. These furrows may reflect splitting of external peptidoglycan as the outer glycan strands are pulled apart along the axis of the cylindrical cell (see below) or uneven peptidoglycan deposition on the inner face.

Concerning periplasmic spaces, the lack of any gap between the inner membrane and cell wall in our cryotomograms contradict the results of previous studies using high-pressure freezing electron cryo-microscopy(Matias and Beveridge 2005), possibly because here we did not pressurize cells or expose them to the osmotic upshock of cryoprotectants. We have, however, observed periplasmic spaces previously in a different (also plunge-frozen) Gram-positive bacterium(Osman et al. 2007). The Gram-positive periplasm may therefore be dynamic: the cell wall appears to be fairly rigid, but the volume of the cell inside may vary in response to buffer conditions and/or pressure, at times opening up a periplasmic space.

Additional imaging, biochemical, and modeling experiments were needed to distinguish between the “circumferential” and “perpendicular” models. One important observation was that ripped sacculi were seen to curl tightly around their outer surfaces. Such curling was to be expected based on previous work which has strongly suggested that new peptidoglycan is incorporated into the inner face of the sacculus while the outer face of the sacculus is broken down by autolysins(Koch and Doyle 1985). New peptidoglycan is created in a presumably relaxed conformation, but as it matures and moves outwards, it takes on the stress of cell

turgor pressure when the layers above it are degraded. Curling can then be explained as tension relief through contraction of the stressed outer layers, resulting in curls around the outer surface as seen in the tomograms (Figure 2C). Incidentally, another reason to disfavor the perpendicular model as originally proposed (long glycan strands being inserted into vertical gaps within the sacculus all at once) is that it does not explain the need for autolysins(Lovering, Safadi, and Strynadka 2012).

Demonstrating these ideas, the two computational models assembled in an “inside-to-outside” fashion (the circumferential model and the incremental perpendicular model) both exhibited curling when allowed to relax (Figure 3A,C). The all-at-once perpendicular assembly model, however, did not exhibit curling (Figure 3B), and so can be ruled out. Inside-to-outside growth also explains the circumferential ridges that were previously interpreted as coiled cables: as mentioned above, these circumferential textures may be fissures in the exterior of the sacculus caused by degradation of peptidoglycan by autolysins and subsequent tension release. Alternatively, they may be a result of uneven deposition of peptidoglycan upon the inner face.

To differentiate between the remaining circumferential and incremental perpendicular models, we noted that only simulation of the circumferential model predicted a thickening of the sacculus during curling. In contrast, the incremental perpendicular model is braced vertically by inelastic glycan strands, and therefore cannot thicken. Inspection of both strained and relaxed peptidoglycan using ECT revealed that relaxed peptidoglycan does indeed tend to be thicker than strained peptidoglycan, uniquely consistent with the circumferential model. Furthermore, the incremental perpendicular glycan model predicts that the density of peptidoglycan decreases towards the exterior, but real sacculi appeared uniformly dense in the tomograms (Figure 1), again consistent with the circumferential model. Simulations revealed that his uniformity arises because outer glycan strands are pulled back against interior glycan strands by stretched elastic peptide linkages. No such compression is observed in perpendicular models because all peptide bonds are in the plane of the sacculus sheet.

Additional confirmation of the circumferential model came from our observations of the tearing and denaturation of sacculi. In the circumferential model, the peptide crosslinks run parallel to the long-axis of the cell, but in perpendicular models, the peptides appear in essentially all directions within the plane of the sacculus. The direction of tears was highly anisotropic, however, almost always oriented circumferentially around the long axis of the sacculus (see Figure 2). This is only to be expected in the circumferential model, since there would be no preferred direction in the perpendicular models. To further test the hypothesis that peptides are preferentially oriented parallel to the long axis (as they are in the circumferential model but none of the others), we examined denatured sacculi. We suspected that these sacculi would dilate exclusively along their long axis due to disruption of peptide crosslink secondary structure. In contrast, perpendicular and coiled cable models, which have peptides oriented in all directions, predict isotropic dilation. As expected, electron cryo-microscopy showed that sacculi elongate but do not widen when denatured, a result consistent only with the circumferential model (Figure 5).

In sum, these results lead us to conclude that the basic architecture of Gram-positive sacculi is the same as that of Gram-negative sacculi, i.e. the glycan strands are circumferential, crosslinked by peptides running approximately parallel to the long axis of the cell. We further conclude that this architecture is assembled inside-to-outside (i.e. through deposition of glycan strands on the inner face of the sacculus and degradation of the outer surface).

That sacculus architecture is conserved across bacteria is not surprising: Gram-negative and Gram-positive species use the same chemical building blocks, anabolic synthesis pathways, and assembling penicillin binding proteins. Furthermore the guiding Mre proteins behave in a similar manner, with recent studies showing that MreB, an actin homolog implicated as a determinant of rod shape in Gram-negative and Gram-positive bacteria, circles the cell circumferentially around the long axis in both(Garner et al. 2011; Domínguez-Escobar et al. 2011; van Teeffelen et al. 2011). Finally, we have observed remodelling of a thin Gram-negative sacculus into a thick form and back during sporulation and germination of the firmicute *Acetonema longum* (Tocheva et al. 2011) and remodelling of a thick Gram-positive sacculus into a thin form and back during formation of the *B. subtilis* sporulation septum (Tocheva and Jensen et al., "Peptidoglycan transformations during Bacillus subtilis sporulation," co-submitted). This further strongly suggests that the two layers must have the same basic architecture, since they can be gradually interconverted.

Experimental procedures

Sample preparation

Bacillus subtilis strains 168 or Py79 cells were grown in LB to OD_{600} ~ 0.6. Next, 50 ml cultures were cooled to 4°C and pelleted by centrifuging at 5000g for 15 minutes a 4°C. Pellets were resuspended in 12ml 100nM NaCl at 4°C and added dropwise to 10ml 4% SDS pre-heated to 80°C in a water bath with constant stirring. Upon completion, an additional 10ml 8% SDS pre-heated to 80°C was added and the suspension was heated to 80°C for one hour. Crude sacculus preparations were washed by five alternate centrifugation (43000g, 30 minutes; room temperature) and resuspension (in 300ml H_2O). The final pellet was resuspended in 9ml 10mM phosphate buffer at pH 7.8. Sacculi were enzymatically treated by incubation for 30 minutes at 30°C with 10mM MgSO4 and 10μg/ml DNase I. Sacculi were then moved to a shaker at 30°C followed by Rnase A (20 μg/ml for 30 minutes) and trypsin (1mg/ml overnight) treatments. Sacculi were subsequently centrifuged at 43000g for 30 minutes and the pellet was resuspended in 2ml 4% SDS at 95°C and added to 8ml 4% SDS at 95°C for 30 minutes with stirring. 20ml H_2O was added to the suspension and centrifuged at 43000g for 30 minutes at room temperature. The pellet was resuspended in 30ml H_2O with 10mM EDTA and pelleted at 43000g for 30 minutes. The pellet was subsequently resuspended in 30ml H_2O and centrifuged four additional times. Teichoic acids were removed from purified sacculi by incubation in 5% trichloroacetic acid at 4°C for 45 hours followed by incubation in 10% trichloroacetic acid for 10 minutes at 90°C. Sacculi were washed and resuspended five times and resulting pellets of purified sacculi were resuspended and stored at −80°C. Sacculi were fragmented by 3 passages (10s, 6.5m/s) in an MPBio FastPrep-24 homogenizer (MP Biomedicals, LLC, Santa Ana, California) Denatured was conducted by addition of sacculi resuspended in H_2O to a final composition of 7.2M urea, 3.6% trehalose, and 90mM CAPS, pH 10.5.

Electron cryo-tomography and analysis

Sacculi suspensions were mixed with 5x BSA/colloidal gold solution (Ted Pella, Redlands, CA). 4 μl cell suspension was deposited on C-flat 2/2 grids (Protochips, Raleigh, NC) that had been glow-discharged for four minutes, blotted, and plunge-frozen into a liquid ethane/propane mixture using a Vitrobot (FEI Company, Hillsboro, OR) and stored in liquid nitrogen until imaging. Tilt series of whole cells were collected using Leginon(Suloway et al. 2009) or UCSF Tomo(Zheng, Sedat, and Agard 2010) on a 300 kV FEI Polara G2 electron cryo-TEM (FEI Company, Hillsboro, OR) using total dose of approximately 200 $e^{-}/Å^2$, −6 μm defocus, and a tilt range of −64° to +64° with 1° tilt increments at nominal magnification of 27500x and binned 4x using a 4K x 4K Gatan UltraCam to generate final 1Kx1K images with 1.56 nm x 1.56 nm pixels. Tilt series were aligned using either

RAPTOR(Amat et al. 2008) or IMOD(Kremer, Mastronarde, and McIntosh 1996), low-pass filtered to ~10 nm resolution and reconstructing using the tomo3d implementation of the SIRT algorithm(Agulleiro and Fernandez 2011). The sacculus segmentation in Figure 2 was a dual-tilt dataset segmented using Amira (VSG, Burlington, MA). Sacculus thickness was obtained by identifying strained and relaxed peptidoglycan and tracing their interior and exterior surfaces. Subsequent closest distances were calculated between the two sides of the sacculus. Results across 19 sacculi were merged and plotted. Lengths and widths of sacculi and denatured sacculi were obtained from 2-D projection images; lengths and widths were manually identified in all complete sacculi in the field of view of the image and plotted as a scatterplot.

Model building and molecular dynamics

For all models, peptidoglycan strands were first constructed individually from their constituent glycan and peptide residues. For those residues not already present in the CHARMM force field(MacKerell et al. 1998), parameters were derived by analogy to existing ones or through quantum chemical calculations. Individual strands were then placed in a parallel sheet or perpendicular lattice, depending on the model under construction, with initial spacing random, but on average 2 nm apart. For the circumferential model, the peptidoglycan fragment was grown from inside to outside over six cycles. Beginning with a sheet containing 12 strands, 5–8 strands were deposited below the innermost layer at a constant density in each cycle and at varying heights. During an initial 1-ns simulation, peptides were crosslinked with a non-zero probability when they first approached one another such that a crosslinking rate of 50% was maintained(Roten et al. 1994). These links occurred with both new and old peptidoglycan, ensuring that the fragment was continuous throughout its thickness. After equilibration of the newly crosslinked strands, the fragment was stretched by 20% of its original length, such that by the end of the last cycle the peptidoglycan fragment was twice as long as initially, i.e., the oldest strands at the outermost surface were 4 nm apart. Each stretching simulation was divided into 20 discrete steps, each step expanding the unit cell length by only a small fraction and then equilibrating it for 0.1 ns. In all simulations during construction, the fragment was periodic along the cell's long axis, including peptide crosslinks, mimicking an effectively infinite peptidoglycan sheet under tension. Perpendicular models were constructed using a similar algorithm, except that three cycles of new strand deposition, crosslinking, and stretching were used for the inside-to-outside growth model, while only one cycle was required for the model possessing a constant strand density throughout. In total, between 10 and 22 ns of simulation were needed for all stages of each model's construction.

All simulations were carried out with the molecular dynamics software NAMD 2.9(Phillips et al. 2005) at a temperature of 310 K. To reduce the computational cost of simulating the largely porous peptidoglycan fragments, a generalized-Born implicit solvent was utilized(Tanner et al. 2011); system sizes ranged from 75,000 to 113,000 atoms at the end of construction. For relaxation of the sheared fragments, bonds crossing the periodic boundary along the cell long axis were severed and the resulting isolated system simulated for 10–15 ns (see Figure 3). All subsequent visualization and analysis was carried out using VMD(Humphrey, Dalke, and Schulten 1996).

Changes in thickness were calculated based on the change in distance between pairs of NAM glycan residues on the top and bottom surfaces before and after relaxation. A grid of 40Å x 40Å boxes was superimposed upon strained peptidoglycan in the plane of the sheet. For each box, the pairwise distances for all NAM residues were calculated, and the maximally separated pair was chosen to judge change in thickness of the peptidoglycan in that box. Fractional change in thickness was calculated for each pair, and subsequently every

column of boxes in the Y-axis was averaged and plotted (each column therefore representing a different position along the long axis of the cell).

Supplementary Material

Refer to Web version on PubMed Central for supplementary material.

Acknowledgments

We would like to thank Simon Foster for an initial gift of purified *B. subtilis* sacculi and the laboratory of Doug Rees for use of the MPBio FastPrep-24. This work was funded by National Institute of Health grant R01 GM062342 to B.R., an Argonne Director's Postdoctoral Fellowship (J.C.G.), the Howard Hughes Medical Institute, and the Gordon and Betty Moore Center for Integrative Study of Cell Regulation at Caltech. Simulations were carried out with resources provided by the Computation Institute and the Biological Sciences Division of the University of Chicago and Argonne National Laboratory, under grant S10 RR029030-01. We would also like to thank Brigitte Ziervogel for helpful comments on the manuscript.

Bibliography

Agulleiro JI, Fernandez JJ. Fast Tomographic Reconstruction on Multicore Computers. Bioinformatics (Oxford, England). 2011 Feb 15; 27(4):582–583.10.1093/bioinformatics/btq692

Amat, Fernando; Moussavi, Farshid; Comolli, Luis R.; Elidan, Gal; Downing, Kenneth H.; Horowitz, Mark. Markov Random Field Based Automatic Image Alignment for Electron Tomography. Journal of Structural Biology. 2008 Mar; 161(3):260–275.10.1016/j.jsb.2007.07.007 [PubMed: 17855124]

Burge RE, Fowler AG, Reaveley DA. Structure of the Peptidoglycan of Bacterial Cell Walls. I. Journal of Molecular Biology. 1977 Dec 25; 117(4):927–953.10.1016/S0022-2836(77)80006-5 [PubMed: 606839]

Chen, Songye; McDowall, Alasdair; Dobro, Megan J.; Briegel, Ariane; Ladinsky, Mark; Shi, Jian; Tocheva, Elitza I., et al. Electron Cryotomography of Bacterial Cells. Journal of Visualized Experiments: JoVE. 2010. http://www.ncbi.nlm.nih.gov/pubmed/20461053

Cheng KJ, Costerton JW. Ultrastructure of Butyrivibrio Fibrisolvens: a Gram-positive Bacterium. Journal of Bacteriology. 1977 Mar 1; 129(3):1506–1512. [PubMed: 845122]

Dmitriev B, Toukach F, Ehlers S. Towards a Comprehensive View of the Bacterial Cell Wall. Trends in Microbiology. 2005 Dec; 13(12):569–574. [PubMed: 16236518]

Domínguez-Escobar, Julia; Chastanet, Arnaud; Crevenna, Alvaro H.; Fromion, Vincent; Wedlich-Söldner, Roland; Carballido-López, Rut. Processive Movement of MreB-Associated Cell Wall Biosynthetic Complexes in Bacteria. Science (New York, NY). 2011 Jun 2. http://www.ncbi.nlm.nih.gov/pubmed/21636744

Gan, Lu; Chen, Songye; Jensen, Grant J. Molecular Organization of Gram-negative Peptidoglycan. Proceedings of the National Academy of Sciences. 2008 Dec 2; 105(48):18953–18957.10.1073/pnas.0808035105

Gan, Lu; Jensen, Grant J. Electron Tomography of Cells. Quarterly Reviews of Biophysics. 2012; 45(01):27–56.10.1017/S0033583511000102 [PubMed: 22082691]

Garner, Ethan C.; Bernard, Remi; Wang, Wenqin; Zhuang, Xiaowei; Rudner, David Z.; Mitchison, Tim. Coupled, Circumferential Motions of the Cell Wall Synthesis Machinery and MreB Filaments in B. Subtilis. Science (New York, NY). 2011 Jun 2. http://www.ncbi.nlm.nih.gov/pubmed/21636745

Ghuysen JM. Use of Bacteriolytic Enzymes in Determination of Wall Structure and Their Role in Cell Metabolism. Bacteriological Reviews. 1968 Dec 1; 32(4 Pt 2):425–464. [PubMed: 4884715]

Hanaki H, Kuwahara-Arai K, Boyle-Vavra S, Daum RS, Labischinski H, Hiramatsu K. Activated Cell-Wall Synthesis Is Associated with Vancomycin Resistance in Methicillin-Resistant Staphylococcus Aureus Clinical Strains Mu3 and Mu50. Journal of Antimicrobial Chemotherapy. 1998 Aug 1; 42(2):199–209.10.1093/jac/42.2.199 [PubMed: 9738837]

Hayhurst, Emma; Kailas, Lekshmi; Hobbs, Jamie; Foster, Simon. Cell Wall Peptidoglycan Architecture in Bacillus Subtilis. Proceedings of the National Academy of Sciences. 2008; 105(38):14603–14608.

Humphrey W, Dalke A, Schulten K. VMD: Visual Molecular Dynamics. Journal of Molecular Graphics. 1996 Feb; 14(1):33–38. 27–28. [PubMed: 8744570]

Koch AL, Doyle RJ. Inside-to-outside Growth and Turnover of the Wall of Gram-positive Rods. Journal of Theoretical Biology. 1985 Nov 7; 117(1):137–157. [PubMed: 3935878]

Koch AL, Woeste S. Elasticity of the Sacculus of Escherichia Coli. Journal of Bacteriology. 1992 Jul 1; 174(14):4811–4819. [PubMed: 1624468]

Kremer JR, Mastronarde DN, McIntosh JR. Computer Visualization of Three-dimensional Image Data Using IMOD. Journal of Structural Biology. 1996 Jan; 116(1):71–76. [PubMed: 8742726]

Lovering, Andrew L.; Safadi, Susan S.; Strynadka, Natalie CJ. Structural Perspective of Peptidoglycan Biosynthesis and Assembly. Annual Review of Biochemistry. 2012; 81(1):451–478.10.1146/annurev-biochem-061809-112742

MacKerell, D Bashford; Bellott, Dunbrack; Evanseck, JD.; Field, MJ.; Fischer, S., et al. All-Atom Empirical Potential for Molecular Modeling and Dynamics Studies of Proteins†. The Journal of Physical Chemistry B. 1998 Apr 1; 102(18):3586–3616.10.1021/jp973084f

Matias, Valério; Beveridge, Terry. Cryo-electron Microscopy Reveals Native Polymeric Cell Wall Structure in Bacillus Subtilis 168 and the Existence of a Periplasmic Space. Molecular Microbiology. 2005 Apr; 56(1):240–251. [PubMed: 15773993]

Meroueh SO, Bencze KZ, Hesek D, Lee M, Fisher JF, Stemmler TL, Mobashery S. Three-dimensional Structure of the Bacterial Cell Wall Peptidoglycan. Proc Natl Acad Sci U S A. 2006 Mar 21; 103(12):4404–4409. [PubMed: 16537437]

Osman, Shariff; Moissl, Christine; Hosoya, Naofumi; Briegel, Ariane; Mayilraj, Shanmugam; Satomi, Masataka; Venkateswaran, Kasthuri. Tetrasphaera Remsis Sp. Nov., Isolated from the Regenerative Enclosed Life Support Module Simulator (REMS) Air System. International Journal of Systematic and Evolutionary Microbiology. 2007 Dec; 57(Pt 12):2749–2753.10.1099/ijs.0.65137-0 [PubMed: 18048719]

Phillips JC, Braun R, Wang W, Gumbart J, Tajkhorshid E, Villa E, Chipot C, Skeel RD, Kalé L, Schulten K. Scalable Molecular Dynamics with NAMD. J Comput Chem. 2005; 26:1781–1802. [PubMed: 16222654]

Roten CAH, Pagni M, Margot P, Touri F, Karamata D. Specific Labeling of Diaminopimelate: A Radioassay for the Determination of the Peptidoglycan Cross-Linking Index. Analytical Biochemistry. 1994 Dec; 223(2):208–211.10.1006/abio.1994.1575 [PubMed: 7887465]

Suloway, Christian; Shi, Jian; Cheng, Anchi; Pulokas, James; Carragher, Bridget; Potter, Clinton S.; Zheng, Shawn Q.; Agard, David A.; Jensen, Grant J. Fully Automated, Sequential Tilt-series Acquisition with Leginon. Journal of Structural Biology. 2009 Jul; 167(1):11–18.10.1016/j.jsb.2009.03.019 [PubMed: 19361558]

Tanner, David E.; Chan, Kwok-Yan; Phillips, James C.; Schulten, Klaus. Parallel Generalized Born Implicit Solvent Calculations with NAMD. Journal of Chemical Theory and Computation. 2011 Nov 8; 7(11):3635–3642.10.1021/ct200563j [PubMed: 22121340]

Van Teeffelen, Sven; Wang, Siyuan; Furchtgott, Leon; Huang, Kerwyn Casey; Wingreen, Ned S.; Shaevitz, Joshua W.; Gitai, Zemer. The Bacterial Actin MreB Rotates, and Rotation Depends on Cell-wall Assembly. Proceedings of the National Academy of Sciences. 2011; 108(38):15822–15827.10.1073/pnas.1108999108

Tocheva, Elitza I.; Matson, Eric G.; Morris, Dylan M.; Moussavi, Farshid; Leadbetter, Jared R.; Jensen, Grant J. Peptidoglycan Remodeling and Conversion of an Inner Membrane into an Outer Membrane During Sporulation. Cell. 2011 Sep 2; 146(5):799–812.10.1016/j.cell.2011.07.029 [PubMed: 21884938]

Verwer RW, Nanninga N, Keck W, Schwarz U. Arrangement of Glycan Chains in the Sacculus of Escherichia Coli. J Bacteriol. 1978; 136:723–729. [PubMed: 361720]

Vollmer W, Blanot D, de Pedro MA. Peptidoglycan Structure and Architecture. FEMS Microbiol Rev. 2008; 32:149–167. [PubMed: 18194336]

Vollmer, Waldemar; Seligman, Stephen J. Architecture of Peptidoglycan: More Data and More Models. Trends in Microbiology. 2010 Feb; 18(2):59–66.10.1016/j.tim.2009.12.004 [PubMed: 20060721]

Wachi M, Matsuhashi M. Negative Control of Cell Division by mreB, a Gene That Functions in Determining the Rod Shape of Escherichia Coli Cells. Journal of Bacteriology. 1989 Jun 1; 171(6):3123–3127. [PubMed: 2656641]

Young KD. The Selective Value of Bacterial Shape. Microbiol Mol Biol Rev. 2006; 70:660–703. [PubMed: 16959965]

Zheng, Shawn Q.; Sedat, JW.; Agard, DA. Cryo-EM Part A Sample Preparation and Data Collection. Vol. 481. Academic Press; 2010. Chapter Twelve - Automated Data Collection for Electron Microscopic Tomography; p. 283-315.http://www.sciencedirect.com/science/article/pii/S0076687910810122

Summary

How organisms give themselves shape is a fundamental question in biology. Many bacteria grow as hemisphere-capped cylinders of similar size and shape over hundreds of generations. The “Gram-positive” bacteria (which cause major diseases) give themselves shape by coating themselves in a thick layer of peptidoglycan: relatively stiff strands of sugars which are crosslinked into a network by relatively flexible peptides. Yet to understand how this gives them shape we need to know the architecture of the the sugars and peptides, which is as-yet unanswered because the structure is too disordered and big for conventional structural biology techniques, yet too small for light microscopy and other methods. Here we use the recent development of electron cryo-tomography to image purified peptidoglycan in 3-D. Although we could not visualize the architecture of this sugar and peptide network, our images were of high-enough detail to see some distinctive behavior by the peptidoglycan. By computationally simulating a variety of possible underlying architectures, we realized that only one of those architectures could explain these distinctive behaviors. Together with results from previous work, this rules out other models, and strongly supports a model in which the sugar strands run around the long-axis of the cell.

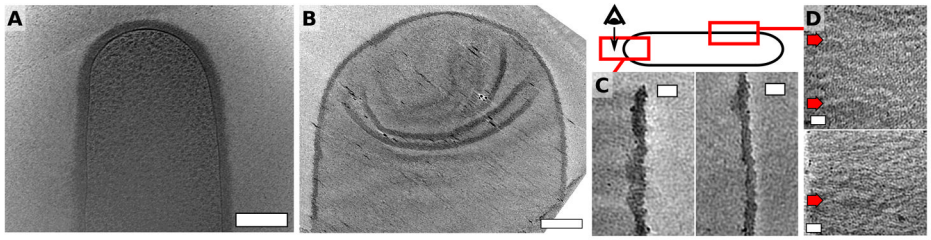

Figure 1. Peptidoglycan texture and density is homogenous in cross-sections in cryo-tomograms of both intact cells and purified sacculi

(A) Tomographic slice through a live *B. subtilis ΔponA* mutant (a mutant that is thinner than wild-type *B. subtilis* and thus ammenable to ECT). Scalebar, 200 nm (B) Tomographic slice through an isolated wild-type *B. subtilis* sacculus. Scalebar, 250 nm (C) Two representative tomographic cross-sections across the wall of isolated *B. subtilis* sacculi perpendicular to the viewing plane reveal a globally straight sacculus side-wall with local variations in thickness. In both tomographic slices the sacculus interior is to the left. (D) Two representative top-down slices through tomograms parallel to the plane of the sacculus illustrating surface textures (red arrows) previously interpreted to be the surfaces of coiled cables composed of helical coils of peptidoglycan. In both tomography slices the long axis of the cell runs vertically. Scale bars 50nm.

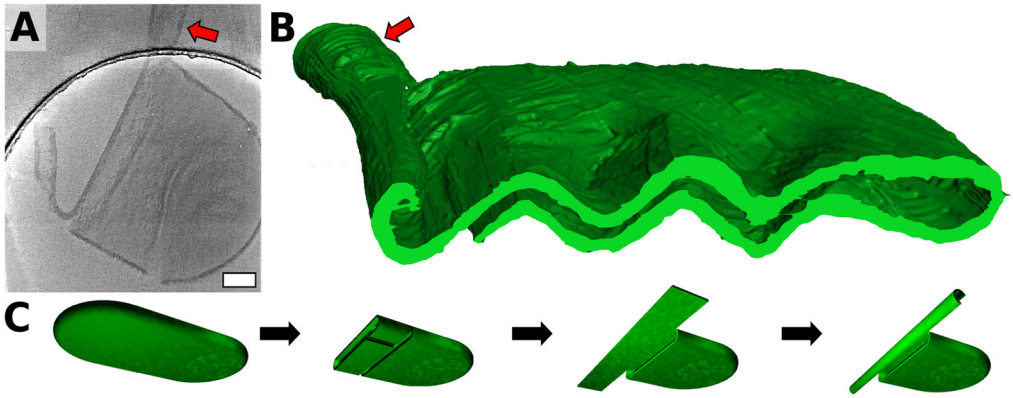

Figure 2. Fragmented sacculi consistently curl up around their outer surface and exhibit a preferential tearing direction

(A) 20 nm-thick slice through the X-Y plane of a fragmented sacculus reconstructed from dual-axis tilt series data. Bar, 200 nm. Red arrow highlights the curling seen in relaxed fragmented peptidoglycan. (B) Isosurface rendering of sacculus fragment to illustrate curling of peptidoglycan around its outer face. Red arrow highlights corresponding area of relaxed peptidoglycan shown in Panel (A). (C) Proposed fragmentation mechanism.

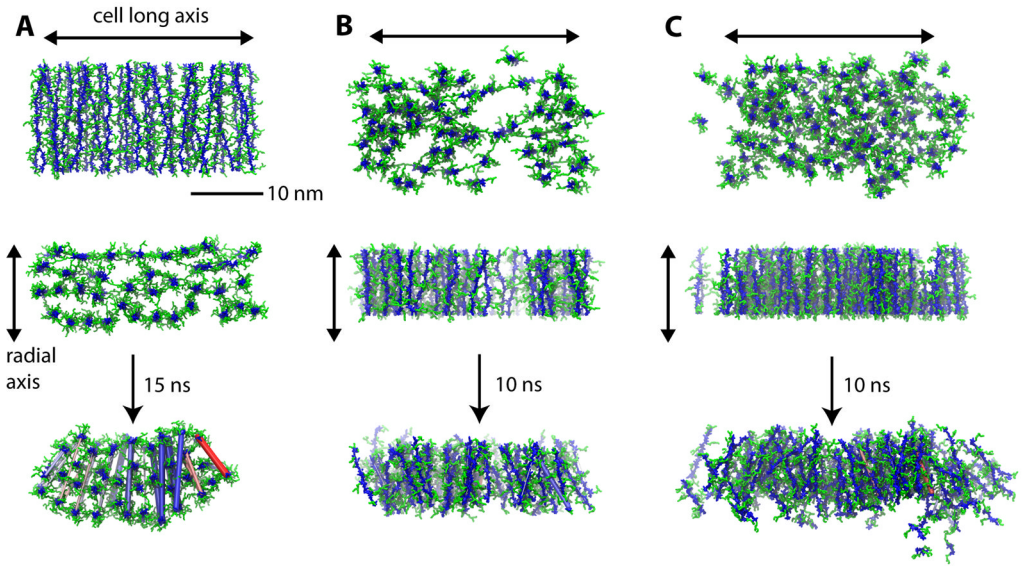

Figure 3. Molecular dynamics of three models of peptidoglycan architecture show that the circumferential model curls and thickens upon relaxation

Assembly of strained peptidoglycan according to three possible models of assembly, and subsequent relaxation. Glycan strands are depicted in blue and peptide crosslinks in green. (A) Relaxation of a circumferential peptidoglycan fragment. Note circumferential peptidoglycan thickens and curls considerably upon relaxation. (B) Peptidoglycan fragment from the all-at-once perpendicular model as originally proposed before and after relaxation. (C) Fragment grown using an inside-to-outside perpendicular assembly model. For all relaxed fragments, colored cylinders represent changes in distances between two NAM residues on the inner and outer surfaces; cylinder diameter and intensity of shading is proportional to change in distance upon relaxation, with red representing contraction and blue representing expansion.

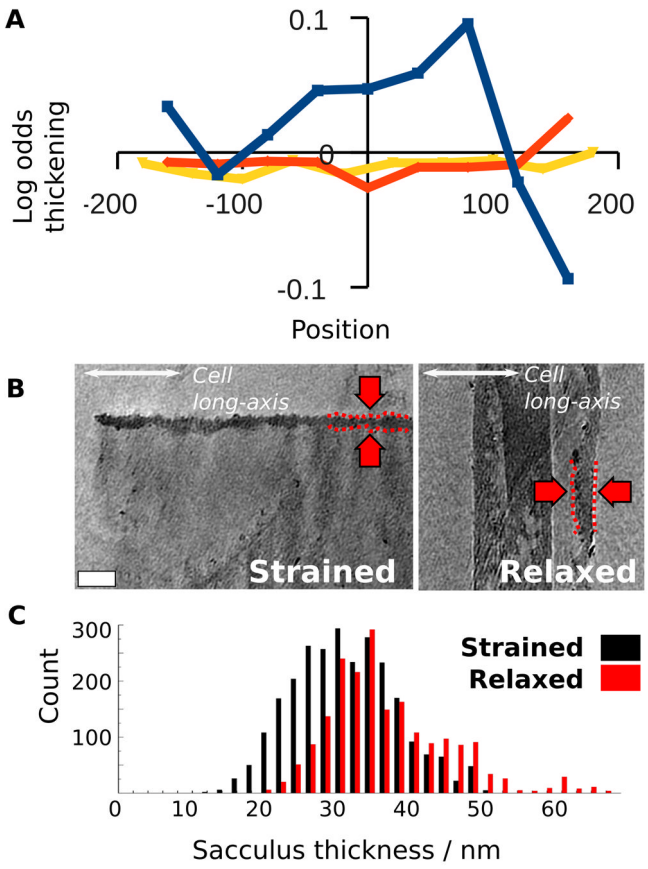

Figure 4. Purified peptidoglycan thickens upon relaxation, an observation accounted for in modeling studies only by the circumferential model

(A) Quantification of thickening observed in molecular dynamics simulations. The log ratio of relaxed to strained thickness (calculated by picking evenly spaced pairs of NAM residues on the inner and outer surfaces) is plotted as a function of position along the original long-axis of the cell, in 40-Å bins. Blue: circumferential, red: perpendicular, yellow: alternative perpendicular models (B) Illustration of measurements of sacculus thickness from both strained and relaxed peptidoglycan (C) Histogram of cross-sections of both relaxed and strained sacculi illustrating thickening of sacculi upon relaxation.

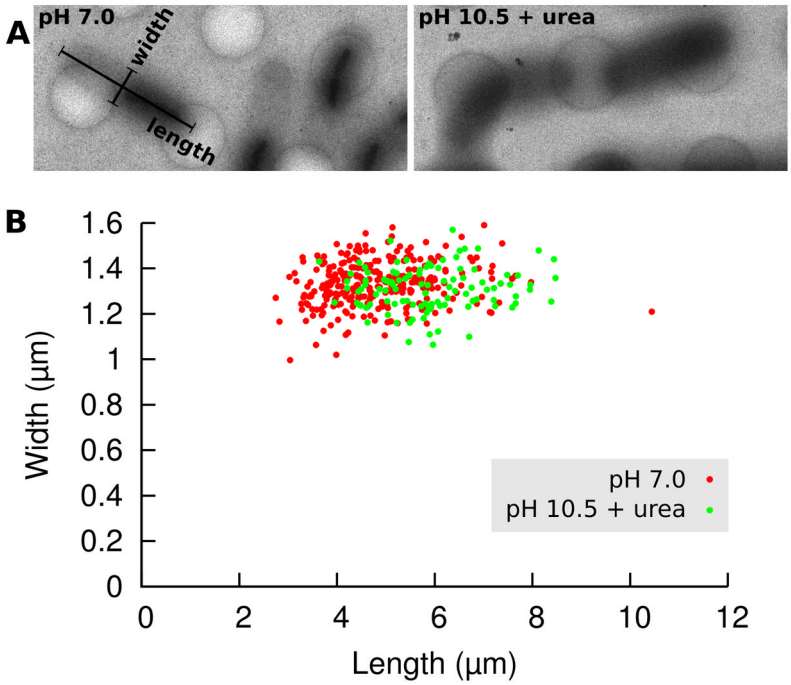

Figure 5. Denatured sacculi elongate but maintain the same width

(A) Projection images of isolated sacculi before and after denaturation. (B) Scatter plot of sacculus length vs. width. Note that the width distribution does not shift whereas the length distribution does.